Journal of Power Sources 244 (2013) 450–455

Contents lists available at SciVerse ScienceDirect

Journal of Power Sources

journal homepage: www.elsevier.com/locate/jpowsour

Lithium insertion into carbon-rich SiOC ceramics: Influence of pyrolysis temperature on electrochemical properties

Jan Kaspar*, Magdalena Graczyk-Zajac, Ralf Riedel

Institut für Materialwissenschaft, Technische Universität Darmstadt, Petersenstr. 32, 64287 Darmstadt, Germany

HIGHLIGHTS

- Carbon-rich SiOC as anode material for Li-ion batteries.
- Influence of pyrolysis temperature (T_{pyr}) on electrochemical properties.
- Different microstructure development with T_{pyr}.
- Increasing carbon organization and Si–O–C network degradation.
- Reducing capacities and changing voltage profiles.

ARTICLE INFO

Article history:
Received 25 October 2012
Received in revised form
21 November 2012
Accepted 23 November 2012
Available online 30 November 2012

Keywords:
Li-ion battery
Anode
Carbon-rich SiOC
Influence of pyrolysis
Temperature
High capacity

ABSTRACT

Carbon-rich silicon oxycarbide ceramics (SiOC) prepared via thermal conversion of polyorganosiloxane demonstrate high lithiation capacity and reliable rate capability when used as anode material in Li-ion batteries. The electrochemical properties of carbon-rich SiOC are strongly related to microstructure and phase composition, dependent on final pyrolysis temperature. Both, the increasing organization of free carbon segregated within the microstructure and the gradual degradation of the amorphous Si–O–C network with increasing pyrolysis temperature (T_{pyr}) lead to reduced capacities and changing voltage profiles. Within our study, the highest registered capacity of 660 mAh g^{-1} for T_{pyr} = 900 °C dropped below 80 mAh g^{-1} for SiOC pyrolyzed at 2000 °C. A continuous decrease in capacity is observed, when increasing T_{pyr} stepwise by 100 °C, which can be explained by major microstructural changes. First, the free carbon within the ceramic microstructure organizes toward higher ordered configurations, as determined by Raman spectroscopy. Second, X-ray powder diffraction demonstrates a decomposition of the amorphous Si–O–C network resulting in SiC crystallization and growth of SiC domains. Simultaneously, FTIR spectroscopy shows a strong increase of Si–C vibration with T_{pyr}, while Si–O vibration diminishes and almost disappears after annealing at 1700–2000 °C. According to our study we find, that i) increasing carbon organization provides less Li-ion storing sites, ii) gradual Si–O–C network decomposition reduces the structural stability of the free carbon phase and iii) formation of electrochemically inactive SiC account for reduced capacities and changing voltage profiles with increasing T_{pyr}.

1. Introduction

Polymer-derived silicon oxycarbide ceramics (SiOC) containing a high amount of free carbon within their microstructure attracted attention as alternative anode material for Li-ion batteries [1–5]. Polymer derived SiOC is synthesized via pyrolysis of polyorganosiloxanes in protective atmosphere by a polymer precursor to ceramic conversion [6]. The lithiation capacity of carbon-rich SiOC is closely related to its microstructure and phase composition. The material consists of an amorphous Si–O–C network in coexistence with an interpenetrating free carbon network [7,8]. In this structure, the segregated carbon serves as Li-ion host, offering a large variety of Li-storing sites due to its disordered nature. Major storing sites are: Edges of graphene sheets, interstitial spaces between graphene layers, micro- and nanopores, graphite nano-crystallites, interfacial and defect sites. On the contrary, the amorphous Si–O–C network plays a stabilizing role toward the free carbon and does not actively contribute to Li-ion storage [1,4,5].

The results presented in this paper are along with our recent study on carbon-rich SiOC anodes derived from a commercial preceramic polymer, namely Polyramic® RD-684a [4,5]. Both studies suggest

* Corresponding author. Tel.: +49 6151 16 6343; fax: +49 6151 16 6346.
E-mail address: kaspar@materials.tu-darmstadt.de (J. Kaspar).

0378-7753/$ – see front matter © 2012 Elsevier B.V. All rights reserved.
http://dx.doi.org/10.1016/j.jpowsour.2012.11.086

an influence of i) the polymer pretreatment and ii) the final pyrolysis temperature on the electrochemical properties of $SiOC_{RD684}$ due to the attained microstructural features. For further clarification a comprehensive sample series was prepared within the temperature range between 900 and 2000 °C and systematically studied by means of XRD, Raman- and IR-spectroscopy and elemental analysis, as well as by electrochemical methods. The characterization of the samples prepared at 1100 and 1300 °C already discussed in reference [5] is for the coherence recalled in the present work. The collected data clearly outline a strong correlation between the final pyrolysis temperature, ceramic microstructure evolution and achievable electrochemical performance.

2. Experimental

2.1. Sample preparation

Ten samples of carbon-rich SiOC were prepared via pyrolysis of polyorganosiloxane Polyramic® RD-684a ($SiOC_{RD684}$, Starfire Systems Inc., USA) in protective atmosphere. Prior to pyrolysis, the polymer-precursors were thermally cross-linked at 400 °C for 3 h. Cross-linking and pyrolysis were carried out under a steady flow of purified argon and heating rates were adjusted to 50 °C h^{-1} for cross-linking and 100 °C h^{-1} for pyrolysis. The final ceramization temperature ranged from 900 to 2000 °C with a holding time of 3 h. For the treatment at 900–1100 °C a horizontal tube-furnace with standard Schlenk-technique was used. Pyrolysis between 1200 and 1700 °C was carried out in a horizontal alumina tube furnace and for the 2000 °C sample an Astro graphite furnace was used. In the following, samples are denoted according to their final pyrolysis temperature (T_{pyr}), e.g. $SiOC_{1100}$.

2.2. Characterization methods

XRD analysis was carried out at a Bruker D8 Advance (Bruker, USA), using Ni-filtered Cu K_α radiation. Mirco-Raman spectra were performed on a confocal micro-Raman spectrometer Horiba HR 800 (Horiba, Japan), using an Ar-Ion laser with a wavelength of 514.5 nm. Infrared spectra were recorded with a Bruker Vertex 70 FT-IR spectrometer (Bruker, USA) in transmission geometry, using KBr pellets. For elemental analysis, a carbon analyzer Leco-200 (Leco Corporation, USA) was used to determine the carbon content and an N/O analyzer Leco TC-436 (Leco Corporation, USA) to determine the oxygen content in the samples. The silicon fraction was calculated as the difference to 100 wt-% of the sum of the wt-% values of carbon and oxygen, assuming a negligibly small amount of hydrogen and no other elements present in the samples.

2.3. Electrode preparation

Pyrolyzed samples ($SiOC_{900}$–$SiOC_{2000}$) were hand-ground to a fine powder and processed in the following way: 85 wt-% sample material (referred to as active mass) were mixed with 5 wt-% Carbon black SuperP® (Timcal Ltd., Switzerland) and 10 wt-% polyvinylidene fluoride (PVdF, SOLEF Solvay, Germany) solved in N-methyl-2-pyrrolidone (NMP, BASF, Germany). The obtained slurry was homogenized and tape casted on the rough side of 10 μm thin copper foil (SECu58, Schlenk Metallfolien GmbH, Germany). Wet-film thickness was adjusted to 130 μm. The loading of active material after solvent evaporation was about 3.3 mg cm^{-2}. Circular electrodes were cut and dried under vacuum in a Buchi oven at 80 °C for 24 h, before transferred to an argon filled glove-box with H_2O/O_2 contamination < 1 ppm (MBraun Glove Box Systems, Germany). Measuring cells of two-electrode Swagelok® type were assembled, using metallic lithium foil (99.9% purity, Alfa Aesar, USA) as reference/counter electrode, 1 M $LiPF_6$ in EC:DMC, ratio 1:1 (LP30, Merck KGaA, Germany) as electrolyte and Whatman™ glass fiber filter (Whatman™, UK) as separator. Hermetically closed cells were connected to a VMP3 multipotentiostat (BioLogic Science Instruments, France) and studied by galvanostatic cycling with potential limitation (GCPL). GCPL measurements were performed between 0.005 and 3 V (E vs. Li/Li^+) at charging/discharging currents of 37, 74 and 372 mA g^{-1}. Within one charging–discharging cycle, the same current rates were applied and capacities were recalculated to the initial amount of active mass.

3. Results and discussion

3.1. X-ray powder diffraction

Fig. 1 presents the X-ray diffraction patterns prior reported for $SiOC_{900}$–$SiOC_{1400}$ [5], completed with samples prepared between 1500–2000 °C. From 900 to 1200 °C the samples remain X-ray amorphous [5], while from 1300 to 2000 °C SiC crystallization is detected in consequence of a carbothermal reaction of silica with carbon [9]. As a result, the amorphous Si–O–C network gradually decomposes. With increasing T_{pyr} from 1300 to 2000 °C, the diffraction intensity related to SiC increases and the signal width gets narrower, indicating growth of SiC domains. At lower temperatures, a weak signal appears at 26.5° related to diffraction at graphitic carbon within the free carbon phase. Furthermore, a broad hump around 43° is recognized, originating from arbitrary diffraction at graphene sheets, characteristic for disordered carbons [10,11]. Except for $SiOC_{2000}$, the graphite reflexes are weak, suggesting the segregated carbon of predominantly amorphous nature. The observed graphitization at 2000 °C is characteristic for disordered soft carbon and emphasizes the increasing carbon organization with T_{pyr} [12,13]. Both findings are in good agreement with the results obtained by Raman and FTIR spectroscopy, discussed in the following sections.

3.2. Raman-spectroscopy

Micro-Raman spectroscopy was performed to further analyze the structural development of the segregated carbon with

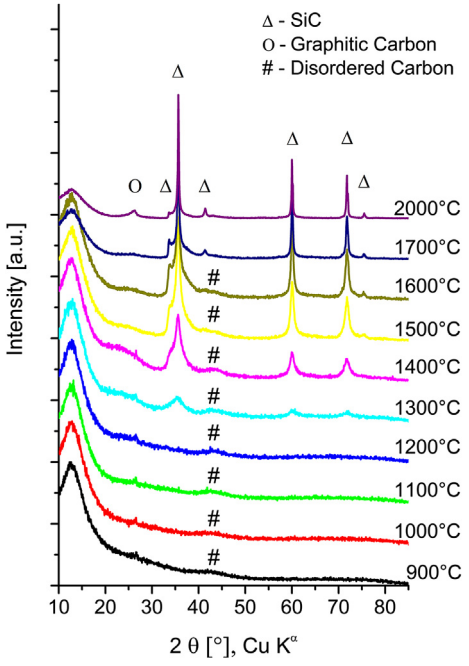

Fig. 1. XRD pattern of the samples SiOC 900–2000 °C.

increasing T_{pyr}. The recorded spectra are shown in Fig. 2. For all temperatures the characteristic carbon vibrations are present: The D-band around 1350 cm^{-1}, the G-band around 1580 cm^{-1}, the 2D vibrations at 2440, 2700 and 3200 cm^{-1} and the D + G combination mode at 2950 cm^{-1}. In all spectra the integral intensity of the D-band $I(A_D)$ is stronger than that of the $I(A_G)$, proving the disordered nature of the segregated carbon. Integral intensities were obtained by Lorentzian fit of D- and G-band within each spectrum [14]. With increasing T_{pyr}, the D- and G-band get more narrow and distinct due to i) a decreasing number of intrinsic defect sites, ii) disappearance of residual C–H bonds present at lower T_{pyr} and iii) vanishing of dangling bonds. Simultaneously, the intensity of the 2D vibrations strongly increases, demonstrating increasing structural carbon organization and graphitization toward 2000 °C [15–19]. In contrast, no trace of the Raman signal from SiC can be detected, probably because of both the relatively low level of SiC segregation and the reduced size of the formed SiC domains [9].

The integral intensities $I(A_D)$ and $I(A_G)$ for each temperature and the dimensions of the corresponding carbon crystallite sizes (L_a), calculated by the general valid equation (Eq. (1)) reported by Cancado et al. [15], with laser wavelength $\lambda = 514$ nm, are summarized in Table 1. The increase in carbon crystallite size with T_{pyr} perfectly matches the found increase in carbon organization by means of Raman 2D bands. The sample $SiOC_{900}$ shows a larger L_a than $SiOC_{1000}$ which is not in agreement with the general trend presented in Table 1. However, for this sample the pyrolysis temperature of 900 °C was most likely too low to eliminate residual C–H bonds within the carbon phase, as suggested by the D-band shoulder toward lower wavenumbers. This so called I-mode is representative for the presence of mixed sp^2–sp^3-hybridized carbon [14].

$$L_a(\mathrm{nm}) = \left(2.4 \times 10^{-10}\right)\lambda^4 \left(\frac{(I(A_D))}{(I(A_G))}\right)^{-1} \quad (1)$$

Eq. (1). Equation used for the estimation of the carbon crystallite size L_a [15].

Table 1
Estimated carbon crystallite size L_a in dependence of T_{pyr}, calculated by Eq. (1).

T_{pyr} [°C]	$I(A_D)$	$I(A_G)$	L_a [nm]
900	134	42	5.25
1000	142	42	4.95
1100	194	58	4.99
1200	143	50	5.86
1300	171	64	6.25
1400	114	47	6.91
1500	102	54	8.87
1600	89	51	9.60
1700	88	51	9.71
2000	71	54	12.74

3.3. FTIR-spectroscopy

Fig. 3 presents the FTIR spectra for $SiOC_{900}$–$SiOC_{2000}$. In all spectra characteristic bands for Si–O and Si–C vibrations are visible, originating from $SiO_{4-x}C_x$ ($x = 1$–4) mixed bonds as building units of the amorphous Si–O–C phase and form crystalline SiC formed at higher annealing temperatures. At 455 cm^{-1} Si–O–Si rocking vibration and around 790 cm^{-1} O–Si–O band bending, overlapping with Si–C stretching vibration at 830 cm^{-1}, is found. The weak absorption at 620 cm^{-1} is also due to Si–C vibration. The broad absorption in the range of 1000–1060 cm^{-1} originates from Si–O, similar to vitreous silica showing absorption at 1090 cm^{-1}. The shift to lower wavenumbers indicates that Si–O bonds are barely located in SiO_4 coordination but rather in random $SiO_{4-x}C_x$ mixed bonds [20–23].

With increasing temperature of pyrolysis the intensity of the Si–O bands at 455 cm^{-1} and 1000–1600 cm^{-1} strongly diminishes. Especially the band at 455 cm^{-1} completely disappears for $SiOC_{1500}$–$SiOC_{2000}$. Simultaneously, a significant intensity increase and a shift of the overlapping Si–O and Si–C vibration around 800 cm^{-1} are found. At 900 °C, the Si–O vibration is dominating with a characteristic absorption maximum at 790 cm^{-1}. But already for the sample annealed at 1300 °C, this maximum is shifted toward

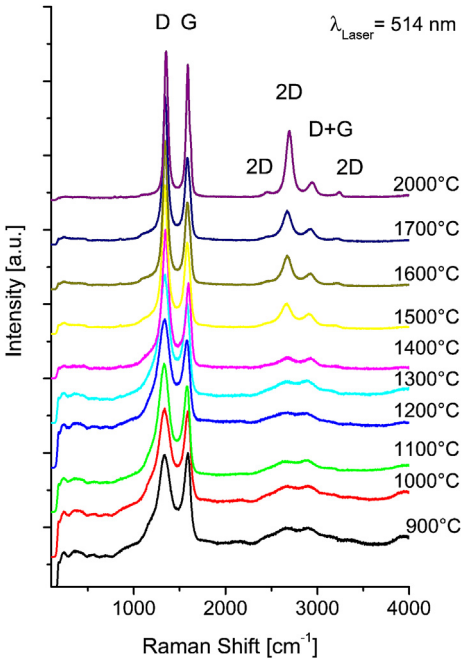

Fig. 2. Raman spectra of the samples SiOC 900–2000 °C.

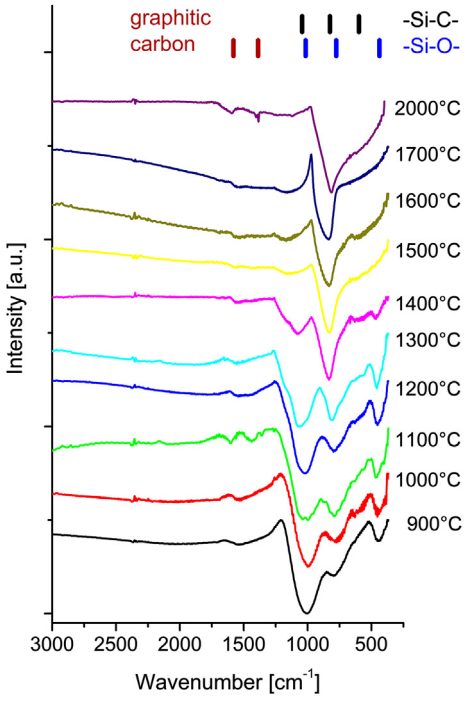

Fig. 3. FTIR spectra of the samples SiOC 900–2000 °C.

830 cm^{-1}, indicating a significant decrease of the Si–O contribution and a strong increase of Si–C vibration. For the samples $SiOC_{1700}$ and $SiOC_{2000}$, Si–C vibration at 830 cm^{-1} and 820 cm^{-1} is detected, exclusively.

The development of the Si–O and Si–C absorption bands with T_{pyr} outlines the progressive degradation of the Si–O–C network, characterized by the disappearance of Si–O intensity and increasing dominance of Si–C vibration. This result well correlates with the found SiC crystallization and SiC domain growth for the samples $SiOC_{1300}$–$SiOC_{2000}$ by means of XRD. For completeness, the bands located at 1350 and 1580 cm^{-1} for $SiOC_{2000}$ are related to graphitic carbon vibration [24].

3.4. Elemental analysis

Table 2 presents the results obtained from elemental analysis for representative samples from the series $SiOC_{900}$–$SiOC_{2000}$. Based on the chemical composition an empirical formula for the SiOC stoichiometry can be derived and the amount of free carbon segregated in the microstructure quantified (see Table 2) [25,26]. For $SiOC_{1000}$–$SiOC_{1400}$, the chemical composition is similar and the free carbon content is exceptionally high with about 41 wt-%. Up to an annealing temperature of 1300 °C, the amount of oxygen is stable, but starts to diminish significantly beyond 1400 °C due to oxygen outgassing in form of CO and SiO. This decrease in oxygen content illustrates the ongoing Si–O–C decomposition, as analyzed by XRD and FTIR spectroscopy. At 2000 °C almost no oxygen is present anymore. In consequence of the reduced oxygen amount, the carbon and silicon content increases for the samples heat-treated at 1400 °C and higher. On the contrary, the total amount of free carbon drops at higher T_{pyr}, due to the loss of CO.

3.5. Electrochemical performance

The characteristic first cycle lithiation/delithiation profiles for $SiOC_{900}$–$SiOC_{2000}$ are presented in Fig. 4, all recorded with a current rate of 37 mA g^{-1}. All cycles show significant hysteresis during Li-insertion/extraction with coulombic efficiencies between 61.5% ($SiOC_{1100}$) and 20.5% ($SiOC_{1700}$). The registered reversible capacities diminish with increasing T_{pyr} from 738 mAh g^{-1} for $SiOC_{900}$ to 75 mAh g^{-1} for $SiOC_{2000}$. Table 3 summarizes the measured values for the first charging capacity (C_{ch}), reversible capacity (C_{rev}), irreversible capacity (C_{irr}) and corresponding coulombic efficiency (η). The columbic efficiency has been calculated as the ratio $C_{rev}/C_{ch} \times 100\%$. The electrochemical behavior of the samples $SiOC_{1100}$ and $SiOC_{1300}$ has already been discussed in [5] within the context of the advantages of various cross-linking methods [4,5]. The potential vs. capacity curves for the mentioned samples are re-called in Fig. 4 for its completeness.

In general, voltage profiles for $SiOC_{900}$–$SiOC_{1500}$ appear quite similar, showing a long sloping plateau between 0.4–0.005 V in the cathodic branch, which is related to Li-ion storage in the disordered carbon phase. In the anodic branch, most of the charge is continuously recovered below 1.5 V ($SiOC_{900}$–$SiOC_{1400}$). Similar voltage profiles were reported for carbon-rich SiOC and disordered soft or hydrogen containing carbon [1,4,5,12,27]. Voltage profiles of $SiOC_{1600}$ and $SiOC_{1700}$ appear different, showing an additional plateau at 0.95 V in the cathodic branch, followed by steeply sloping toward 0.5 V and further sloping to 0.005 V. Similar behavior has been reported and discussed for carbon-rich SiCN ceramics pyrolyzed at 2000 °C by Graczyk-Zajac et al. [28]. During the lithium extraction less than 160 mAh g^{-1} of charge is recovered for $SiOC_{1500}$–$SiOC_{1700}$ with coulombic

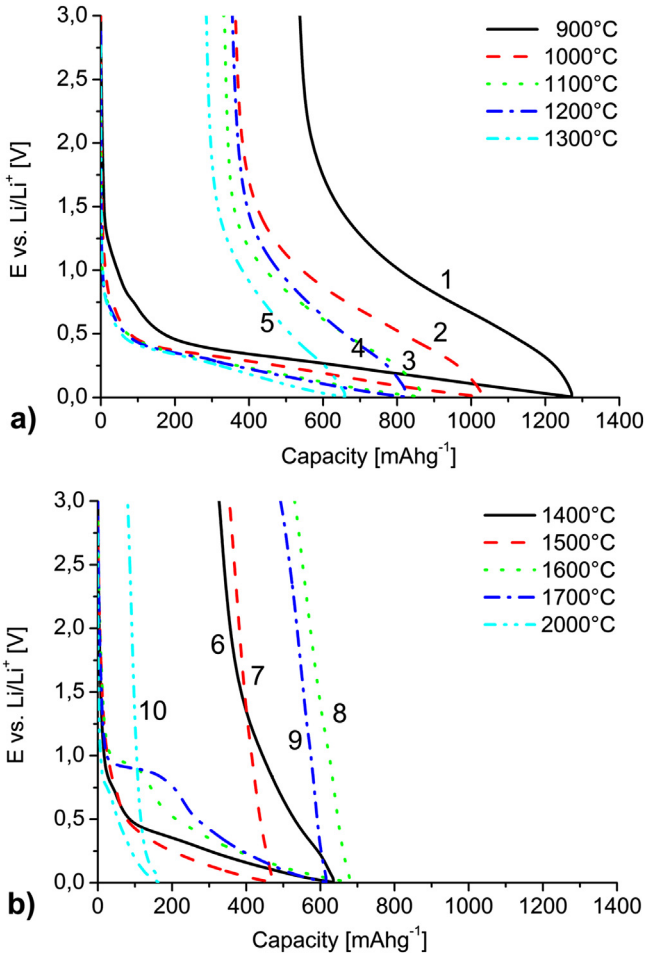

Fig. 4. First cycle lithiation/delithiation profile for SiOC a) 900–1300 °C (curves 1–5) and b) 1400–2000 °C (curves 6–10).

Table 2
Elemental analysis of $SiOC_{RD684}$ prepared upon pyrolysis between 900 °C and 2000 °C (* – normalized to one silicon atom).

T_{pyr} [°C]	Si [wt-%]	O [wt-%]	C [wt-%]	Empirical formula*	Free carbon [wt-%]
900	30.35	22.07	47.58	$SiO_{1.28}C_{3.67}$	42.88
1100	33.25	17.55	49.20	$SiO_{0.93}C_{3.46}$	41.57
1300	33.24	17.65	49.11	$SiO_{0.93}C_{3.46}$	41.52
1400	34.43	14.24	51.33	$SiO_{0.73}C_{3.49}$	41.95
1600	41.26	3.19	55.55	$SiO_{0.14}C_{3.15}$	39.10
2000	43.41	0.04	56.55	$SiC_{3.05}$	38.00

Table 3
Comparison of the first cycle charging capacity, reversible capacity, irreversible capacity and coulombic efficiency for the samples SiOC 900–2000 °C.

T_{pyr} [°C]	C_{ch} [mAh g^{-1}]	C_{rev} [mAh g^{-1}]	C_{irr} [mAh g^{-1}]	η [%]
900	1277	738	539	57.8
1000	1028	614	414	59.7
1100	866	532	334	61.5
1200	828	471	357	56.9
1300	658	374	284	56.8
1400	641	313	328	48.8
1500	471	141	330	29.9
1600	686	154	532	22.4
1700	621	128	493	20.6
2000	163	75	88	46.0

efficiencies < 30%. The sample pyrolyzed at 2000 °C demonstrates the lowest reversible capacity among the studied series (75 mAh g^{-1}), however the cycling efficiency again increases, from 20.6% for $SiOC_{1700}$ to 46.0% registered for $SiOC_{2000}$. Nevertheless, from a practical point of view, the significant hysteresis, low coulombic efficiency and low reversible capacity of the samples prepared between 1500 and 2000 °C clearly disqualifies these samples for battery application.

The registered charging and reversible capacity for the series $SiOC_{900}$–$SiOC_{1500}$ continuously decreases while voltage profiles remain similar. This diminution in charge storage is related to a decrease in available Li-ion storing sites within the free carbon phase. As found by Raman, the structural organization of the free carbon increases with temperature of pyrolysis. According to our previous reports [4,5] and findings of Azuma et al. [13], higher ordered carbons can host less Li-ions than order-less configurations, meaning that at lower T_{pyr} the corresponding capacities must be higher than at higher T_{pyr}.

Fig. 5 summarizes the average reversible capacity registered for $SiOC_{900}$–$SiOC_{2000}$ for continuous cycling at different current rates. The average values are calculated from 10 cycles with a current of 37 mA g^{-1}, 20 cycles with 74 mA g^{-1} and 30 cycles with 372 mA g^{-1}. The error bars in Fig. 5 indicate the standard deviation from the average value. Deviation comes from capacity fading during cycling or, for the samples showing stable cycling behavior ($SiOC_{1000}$, $SiOC_{1200}$) from temperature fluctuations in the laboratory where the cells were tested. Table 4 summarizes the calculated values. Between 900 and 1200 °C, the measured capacities of 666 - 460 mAh g^{-1} for cycling current 37 and 74 mA g^{-1} are much higher than the theoretical capacity of graphite (372 mAh g^{-1}). For $SiOC_{1300}$–$SiOC_{1400}$ the reversible capacity drops below 400 mAh g^{-1} and for the samples $SiOC_{1500}$–$SiOC_{2000}$ capacity of less than 140 mAh g^{-1} is recovered in average.

Among the studied materials, sample $SiOC_{900}$ shows the highest capacity, but also the largest fading during cycling. Within the first ten cycles at 37 mA g^{-1}, the recovered charge diminishes from initially 738 to 644 mAh g^{-1}. In particular between the first and second cycle 40 mAh g^{-1} are lost. Most probably, this decay is related to a large amount of residual hydrogen within the sample, especially within the free carbon phase in form of C–H bonds stemming from the initial polymer precursor. The H-content for a similar prepared sample at 900 °C was analyzed to 1.13 wt-% [29].

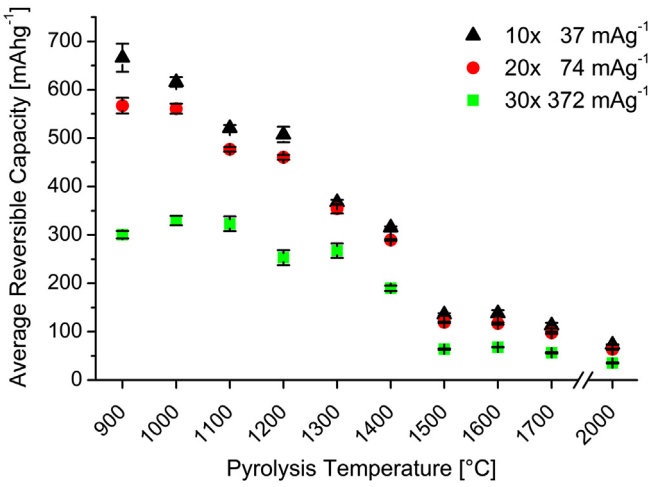

Fig. 5. SiOC average reversible capacity in dependence of temperature of pyrolysis. Average values were calculated from 10 cycles at 37 mA g^{-1}, 20 × 74 mA g^{-1} and 30 × 372 mA g^{-1}. Error bars indicate the standard deviation from the average value.

Table 4
SiOC average reversible capacity in dependence of temperature of pyrolysis, for the current rates: 37, 74 and 372 mA g^{-1}.

T_{pyr} [°C]	Average reversible capacity at the following current rates		
	37 mA g^{-1}	74 mA g^{-1}	372 mA g^{-1}
900	666	567	300
1000	615	561	330
1100	521	477	323
1200	507	460	253
1300	367	354	268
1400	315	289	190
1500	135	120	64
1600	138	117	68
1700	112	97	56
2000	73	64	35

According to Dahn et al., Li-ion storage in H-containing carbons occurs by Li-binding in the vicinity of H atoms [12]. During Li extraction, the original C–H bonds reform. When this reforming is disturbed or incomplete, the cycling capacity slowly decays with continuous cycling [12,30].

Among the investigated sample series, $SiOC_{1000}$ and $SiOC_{1100}$ are the most perspective samples for potential application as anode material. Both present outstanding properties: High capacity in combination with good high rate stability. At 37 and 74 mA g^{-1}, the average reversible capacity of $SiOC_{1000}$ (615 mAh g^{-1}, 561 mAh g^{-1}) is approximately 100 mAh g^{-1} higher than that of the sample $SiOC_{1100}$ (512 mAh g^{-1}, 477 mAh g^{-1}). At a current rate of 372 mA g^{-1}, values are quite similar with 330 and 323 mAh g^{-1}. In general, the good high rate performance of $SiOC_{900}$–$SiOC_{1300}$ can be explained by the intrinsic nanostructure of the ceramics, which kinetically boosts the Li-ions due to shorten diffusion pathways [31–33]. Similar findings were reported for nano-structured, carbon-rich SiCN ceramics [34,35].

To summarize, the registered reversible capacities decrease with temperature of pyrolysis (cf. Fig. 5) by two major contributions: First, increasing structural organization of the segregated free carbon leads to less Li-ion storing sites. Second, continuous degradation of the Si–O–C network reduces the structural stability of the free carbon phase.

4. Conclusions

We demonstrated that the temperature of pyrolysis (T_{pyr}) has a significant impact on the electrochemical properties of carbon-rich, polyorganosiloxane derived SiOC ceramics. In particular the analyzed capacities were found to decrease by structural changes of the free carbon phase from highly disordered toward partially graphitized configurations. In consequence, the number of Li-storing sites diminishes, since higher ordered carbons can host less Li-ions than orderless configurations. Additionally, degradation of the stabilizing Si–O–C network occurs, by a solid state reaction of Si–O bonds with carbon, resulting in SiC crystallization, growth of SiC domains and oxygen-loss. This gradual decomposition reduces the structural stability of the free carbon phase, favoring reduced capacities and changing voltage profiles.

Acknowledgments

The authors acknowledge the financial support by the Deutsche Forschungsgemeinschaft (DFG), Bonn, Germany within SPP1473/JP8 and SFB 595/A4 program. Special thanks to G. Mera, C. Fasel and J.-C. Jaud for their support of the characterization of the materials and helpful discussion.

References

[1] H. Fukui, O. Hisashi, T. Hino, K. Kanamura, Appl. Mater. Interfaces 4 (2010) 998–1008.
[2] H. Fukui, H. Ohsuka, T. Hino, K. Kanamura, J. Power Sources 196 (2011) 371–378.
[3] P. Dibandjo, M. Graczyk-Zajac, R. Riedel, V.S. Pradeep, G.D. Soraru, J. Eur. Ceram. Soc. 32 (2012) 2495–2503.
[4] M. Graczyk-Zajac, L. Toma, C. Fasel, R. Riedel, Solid State Ionics 225 (2012) 522–526.
[5] J. Kaspar, M. Graczyk-Zajac, R. Riedel, Solid State Ionics 225 (2012) 527–531.
[6] P. Colombo, G. Mera, R. Riedel, G.D. Soraru, J. Am. Ceram. Soc. 93 (2010) 1805–1837.
[7] S.J. Widgeon, S. Sen, G. Mera, E. Ionescu, R. Riedel, A. Navrotsky, Chem. Mater. 22 (2010) 6221–6228.
[8] S. Martínez-Crespiera, E. Ionescu, H.-J. Kleebe, R. Riedel, J. Eur, Ceram. Soc. 31 (2011) 913–919.
[9] R. Alonso, G. Mariotto, C. Gervais, F. Babonneau, G.D. Soraru, Chem. Mater. 19 (2007) 5694–5702.
[10] F. Bonino, S. Brutti, M. Piana, S. Natale, B. Scrosati, L. Gherghel, K. Müllen, Electrochim. Acta 51 (2006) 3407–3412.
[11] C.L. Burket, R. Rajagopalan, H.C. Foley, Carbon 46 (2008) 501–510.
[12] J.R. Dahn, T. Zheng, Y. Liu, J.S. Xue, Science 270 (1995) 590–593.
[13] H. Azuma, H. Imoto, S.i. Yamada, K. Sekai, J. Power Sources 81–82 (1999) 1–7.
[14] A. Sadezky, H. Muckenhuber, H. Grothe, R. Niessner, U. Pöschl, Carbon 43 (2005) 1731–1742.
[15] L.G. Cancado, K. Takai, T. Enoki, M. Endo, Y.A. Kim, H. Mizusaki, A. Jorio, L.N. Coelho, R. Magalhaes-Paniago, M.A. Pimenta, Appl. Phys. Lett. 88 (2006) 163106.
[16] M.A. Pimenta, G. Dresselhaus, M.S. Dresselhaus, L.G. Cancado, A. Jorio, R. Saito, Phys. Chem. Chem. Phys. 9 (2007) 1276–1290.
[17] A.C. Ferrari, Solid State Commun. 143 (2007) 47–57.
[18] N. Larouche, B.L. Stansfield, Carbon 48 (2010) 620–629.
[19] M.S. Dresselhaus, A. Jorio, R. Saito, Annu. Rev. Condens. Matter Phys. 1 (2010) 89–108.
[20] G.M. Renlund, S. Prochazka, R.H. Doremus, J. Mater. Res. 6 (1991) 2723–2734.
[21] D. Gupta, B. Awasthy, S.P. Varma, J. Mater. Sci. 28 (1993) 1488–1490.
[22] Q. Liu, W. Shi, F. Babonneau, L.V. Interrante, Chem. Mater. 9 (1997) 2434–2441.
[23] Q.-S. Ma, Z.-H. Chen, W.-W. Zheng, H.-F. Hu, Ceram. Int. 31 (2005) 1045–1051.
[24] R.A. Friedel, G.L. Carlson, J. Phys. Chem. US 75 (1971) 1149–1151.
[25] G.D. Soraru, J. Sol-gel. Sci. Tech. 2 (1994) 843–848.
[26] G.D. Soraru, L. Pederiva, J. Latournerie, R. Raj, J. Am. Ceram. Soc. 85 (2002) 2181–2187.
[27] T. Zheng, W.R. McKinnon, J.R. Dahn, J. Electrochem. Soc. 143 (1996) 2137–2145.
[28] M. Graczyk-Zajac, G. Mera, J. Kaspar, R. Riedel, J. Eur. Ceram. Soc. 30 (2010) 3235–3243.
[29] J. Kaspar et al., unpublished data.
[30] T. Zheng, Q. Zhong, J.R. Dahn, J. Electrochem. Soc. 142 (1995) L211–L214.
[31] C.J. Wen, B.A. Boukamp, R.A. Huggins, W. Weppner, J. Electrochem. Soc. 126 (1979) 2258–2266.
[32] A.S. Arico, P. Bruce, B. Scrosati, J.-M. Tarascon, W. van Schalkwijk, Nat. Mater. 4 (2005) 366–377.
[33] G. Peter, B. Bruce, J.-M. Scrosati, Tarascon, Angew. Chem. Int. Ed. 47 (2008) 2930–2946.
[34] J. Kaspar, G. Mera, A.P. Nowak, M. Graczyk-Zajac, R. Riedel, Electrochim. Acta 56 (2010) 174–182.
[35] L.M. Reinold, M. Graczyk-Zajac, Y. Gao, G. Mera, R. Riedel, Carbon-rich SiCN ceramics as high capacity/high stability anode material for lithium ion batteries, J. Power Sources, Submitted for publication.